Investigation of the Kinetics of a TiO_2 Photoelectrocatalytic Reaction Involving Charge Transfer and Recombination through Surface States by Electrochemical Impedance Spectroscopy

W. H. Leng,*,† Z. Zhang,† J. Q. Zhang,† and C. N. Cao†,‡

Department of Chemistry, Yuquan Campus, Zhejiang University, Hangzhou, 310027, China, and State Key Laboratory for Corrosion and Protection of Metals, Institute of Metal Research, Chinese Academy of Sciences, Shenyang 110016, China

Received: April 8, 2005; In Final Form: May 28, 2005

In this paper, the electrochemical impedance spectroscopy (EIS) mathematical model of TiO_2 photoelectrocatalytic (PEC) reactions involving charge transfer and recombination through surface states was developed. The model was used to study the kinetics of photoelectrocatalytic decomposition of salicylic acid. The model simulation results show that the appearance of two distinguishable semicircles in the EIS response depends on the charging of surface state and light intensity. The experimental results demonstrated that similar phenomena to the theoretical simulation results. The model provides a way to obtain the rate constants for the photoelectrochemical reactions of surface states mediating charge transfer and recombination. The applied potential changes not only the recombination rate constant but also the charge-transfer rate constant. Moreover, the experimental EIS results here and those previous published on PEC degradation reactions can be explained by the present model satisfactorily. The relevance of surface states was discussed briefly. The results demonstrated that EIS is a powerful tool for studying the kinetics of PEC decomposition of organic pollutants on TiO_2 electrodes.

1. Introduction

Over the last few decades, TiO_2 photocatalysis has been demonstrated as a promising alternative to conventional water treatment because it can decompose and even mineralize pollutant and/or undesirable compounds in wastewater.[1−5] Since it needs to separate the spent catalyst particles for the slurry system, a number of reports have dealt with the use of supported photocatalysts, especially the use of conducting materials that allow one to improve the efficiency by bias potential in a photoelectrochemical cell.[2−9]

It is generally accepted that when TiO_2 is exposed to light of energy greater than the band-gap energy, an electron is excited from the TiO_2 valence band. The hole produced is involved in the oxidation of organic substrates, either directly or via the OH radical formed by the reaction with OH^- and/or water adsorbed, while the photogenerated electron must be removed from the particles by transfer to a suitable electron acceptor and/or through the external electrical circuit to the counter electrode.[1,10] Despite the tremendous amount of attention paid to the photocatalytic process from both the applied and fundamental viewpoints, the complete reaction mechanism is not fully understood.[11] For example, since the quantum yields for the photooxidation of organics are low (typically less than 0.1), a key question is what factors limit the efficiency of the photocatalytic process. Those TiO_2/electrolyte interfacial processes are obviously crucial to the operation of a photoelectrochemical system, because they control the interfacial charge transfer and recombination of photogenerated electron and hole pairs. Such processes at photoelectrodes have been the topic of much recent work in the field.[12−22]

Electrochemical techniques provide a powerful method for the study of charge transfer and recombination processes at semiconductor/electrolyte interfaces (SEIs). Steady-state measurements offer limited insights into the mechanisms of photoelectrocatalytic (PEC) reactions.[13] Nonstationary techniques have made major contributions to the understanding of the kinetics and mechanisms of elementary processes involved in PEC reactions at the SEI. The most common types of external perturbation involve changes of illumination intensity or electrode potential. One of the most powerful of these techniques is intensity modulated photocurrent spectroscopy (IMPS) that can be used to measure the rate constants of charge transfer and recombination occurring at the SEI.[14−18] Unfortunately, since there are some experimental difficulties in the modulation of light with short wavelength in a wide frequency range at present, this approach has seldom been used to study such a wide band-gap semiconductor like TiO_2.[20] By contrast, electrochemical impedance spectroscopy (EIS) can also be used to obtain the electrode process occurring at illuminated SEI without such a limitation. In fact, by using EIS various equivalent circuit and mathematical models have been proposed to describe the PEC reactions at the illuminated SEI.[17−27] Surprisingly, little work has been reported on the investigation of the PEC degradation reaction of organic at the TiO_2/electrolyte solution interfaces by EIS except for Liu's[25] and our reports.[26] Recently, Liu et al.[25] have found only one arc on the EIS plane display that had a smaller size corresponding to a faster degradation of sulfosalicylic acid. We found that the PEC degradation rate of aniline was inversely proportional to the value of charge-transfer resistance of photoelectrodes formed by the thermal oxidation

* To whom correspondence should be addressed. E-mail: lengwh @ css. zju. edu. cn.
† Zhejiang University.
‡ Chinese Academy of Sciences.

10.1021/jp051821z CCC: $30.25
Published on Web 07/16/2005

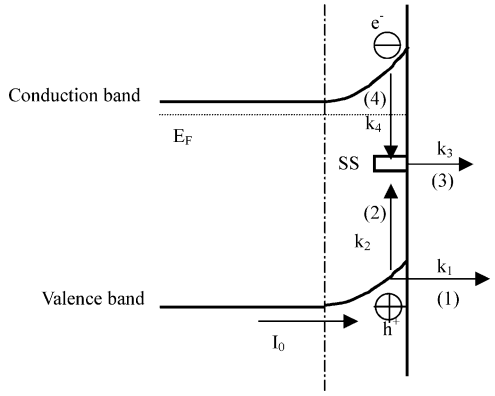

Figure 1. Diagram showing the elementary processes of surface state mediated charge transfer and recombination taking place at the illuminated TiO_2/electrolyte interface.

of titanium.[26] However, all of us failed to explain this phenomenon. More recently, Liu et al.[27] have attempted to use EIS to ascertain the rate-determining step of TiO_2 PEC oxidation of sulfosalicylic acid, where an EIS mathematical model was established to theoretically simulate the PEC reaction. However, they supposed that the applied interfacial potential dropped across the Helmholtz layer, without considering the drop across the depletion layer at the semiconductor side. This treatment is not popular. In fact, many models for the lowly doped semiconductor electrodes supposed that the capacitance of the semiconductor side of the interface was much smaller than that of the Helmholtz layer and most applied potential dropped in the depletion layer.[20,23] Moreover, that time-dependent accumulation of surface charge at the surface may affect, in turn, the redistribution of potential over the depletion and Helmholtz layer and couple to the interfacial kinetics, while this effect is not taken into account for the most of PEC reactions at the semiconductor electrode including TiO_2. In addition, during the early stages of the studies of semiconductor surface processes, the presence of surface states at the interface is commonly believed to be important in dictating the charge-transfer process.[12a,15−18] For example, to account for a high current efficiency (almost 100%) for O_2 evolution during photoelectrolysis of water, a contribution of surface states in charge transfer has been proposed.[12g] However, to our knowledge, the details of the role of surface states at the interface have not been examined in the context of charge transfer in the PEC process of pollutants.

To provide a better interpretation of the EIS results and clearer understanding of the PEC processes at the TiO_2/electrolyte interfaces achieved by measuring the rate constants of the elementary reactions, it is necessary to establish EIS mathematical models. In this paper, an EIS mathematical model of surface states mediating charge transfer and recombination was established, considering that the distribution of the interfacial potential drops over the depletion and Helmholtz layers, and the effect of these on the rate of photogenerated carriers recombination and of electron exchange between the TiO_2 and the redox species in solution. The EIS experimental results can be explained by the present model satisfactorily.

2. EIS Mathematical Model for TiO_2 PEC Reaction

2.1. The Mechanistic Model. We consider surface states of density r (cm^{-2}) located at an energy E_s lower than the Fermi level of the bulk TiO_2 semiconductor. The charge transfer and recombination processes that can be considered are illustrated in Figure 1. The model is developed for the TiO_2/electrolyte interface under anodic bias. On illumination, the photogenerated holes move to the surface. We assume that photogenerated holes move to the surface where they can either transfer directly to any surface complex with the rate constant k_1' (process 1) or be captured by the surface states with the rate constant k_2' (process 2). Holes captured at surface states can also transfer to organics R with the rate constant k_3' (process 3) or recombine with electrons with the rate constant k_4' (process 4). The reversible reaction of process 3 can be neglected if enough anodic bias is applied over the cell; thus it will not be considered in the following. The overall PEC processes on the TiO_2 photoelectrode can therefore be represented as

$$TiO_2 + h\nu \rightarrow (TiO_2{-}h_{VB}^{+})_s + (TiO_2{-}e_{CB}^{-})_s \qquad (1a)$$

$$v_0 = I_0$$

$$h_{VB}^{+} + R \xrightarrow{k_1'} R^{\bullet} \qquad (1)$$

$$v_1 = k_1'[R]p_1 = k_1 p_1$$

$$h_{VB}^{+} + ss^0 \xrightarrow{k_2'} ss^+ \qquad (2)$$

$$v_2 = k_2'[r]p_1 = k_2 p_1$$

$$R + ss^+ \xrightarrow{k_3'} ss^0 + R^{\bullet} \qquad (3)$$

$$v_3 = k_3'[R]p_2 = k_3 p_2$$

$$e_{CB}^{-} + ss^+ \xrightarrow{k_4'} ss^0 \qquad (4)$$

$$v_4 = k_4' n_s p_2 = k_4 p_2$$

where p_1 is the charge density associated with free holes at the surface, p_2 is the corresponding charge density for holes captured by surface states, n_s the electron density at the surface, and I_0 is the current density corresponding to the flux of photogenerated holes toward the surface. All velocities, v, are given in cm^{-2} s^{-1}, and the species in brackets represent the surface concentration of the species in cm^{-2}. This mechanism is identical to that proposed by Hoffmann[1] and others[13,27] if surface states are replaced by OH radicals. Since it is proposed that OH radical is the primary oxidant in most photocatalytic systems,[1,28] the step of holes transferring directly to solution (process 1) will not be considered in the following (for detail analysis see section 4.2). We introduce at this point the shorthand notations $k_1 = k_1'[R]$, $k_2 = k_2'[r]$, $k_3 = k_3'[R]$, $k_4 = k_4' n_s$.

2.2. Assumptions of the Impedance Calculation. In EIS experiments, the illumination intensity is held constant; the flux of holes, I_0, is constant to a good approximation. For simplicity, the potential dependence of I_0 is negligible. This approximation is valid if the penetration depth of the light is smaller than the width of the depletion region.[29] A potential drop ϕ across the TiO_2/electrolyte interface is assumed to consist of two parts, i.e., a potential drop ϕ_{sc} between the bulk of the semiconductor and the semiconductor surface on one hand and a potential drop ϕ_H between the semiconductor surface and the bulk electrolyte, i.e., the potential drop across the Helmholtz layer, on the other hand. A depletion layer usually exists at the semiconductor side of the interface; the differential capacitance of this part of the interface (C_{sc}) is given, most simply, by the Mott−Schottky relation. The capacitance (C_H) of the Helmholtz layer at the electrolyte side of the interface is assumed to be a constant.

Application of an ac potential modulation across the interface changes the potential drops within the depletion and Helmholtz layers. The electrode potential, and hence the surface density of electrons, is modulated. Since the rate of surface recombination depends linearly on the surface concentration of electrons. The potential modulation affects the pseudo-first-order recombination rate constant k_4 that is given by

$$k_4 = k_4' n_s = k_4^\circ \exp\left(\frac{-\alpha q \phi_{sc}}{\kappa T}\right) \tag{5}$$

where α is an ideality factor, q the elementary charge, κ the Boltzmann constant, and T the temperature.

In the following, two cases will be considered. For case A, it is assumed that modulation of the potential drop across the Helmholtz layer does also change the rate constant of charge transfer k_3 by altering the activation energy. In fact, this is considered as the only effect by Liu et al.,[27] who have dealt with the TiO_2/electrolyte interface as that of a metal electrode. Here we assume that the Tafel equation can be used to describe the potential dependence of the rate constant of k_3, thus it is given by

$$k_3 = k_3^\circ \exp\left(\frac{\beta q \phi_H}{\kappa T}\right) \tag{6}$$

where β is charge-transfer coefficient.

For comparison, conversely, in the case of B, it is supposed that this modulation does not change the rate constant k_3. Case A will be the general case in the following unless specified.

The rate constant k_2, which represents the process of holes captured by surface states, is assumed to be independent of potential drop in the depletion layer. The above overall mechanism further implies that photocurrents are not limited by mass transfer.

2.3. Calculation of the EIS. The time-dependent concentrations of charge carriers are described by convention kinetic differential equations. This approach is similar to that taken by Ponomarev et al.[20] The differential equations for the holes are

$$\frac{dp_1}{dt} = I_0 - k_2 p_1 \tag{7}$$

$$\frac{dp_2}{dt} = k_2 p_1 - k_3 p_2 - k_4 p_2 \tag{8}$$

Usually, the variation of potential drop in the depletion should also result in charging of the surface state capacitance, C_{ss}, besides the C_{sc}. If this process is linear and proportional to the potential drop across the depletion layer, it can be described as a charging of C_{ss} through a resistor R_{ss}.[21] The corresponding differential equations are

$$j_{ss} = C_{ss} \frac{d\phi_{ss}}{dt} \tag{9}$$

$$j_{ss} R_{ss} + \phi_{ss} = \phi_{sc} \tag{10}$$

where j_{ss} is the current due to charging the surface state capacitance.

The total time dependent current density through the electrochemical cell is written in two ways. At the semiconductor side of the interface, this current density equals the sum of a faradaic component j^{sc} and a part caused by the charging/discharging of the semiconductor side of the interface.[30] Analogously, the current density at the electrode side of the interface consists of a faradaic component j^H and a part of caused by the charging/discharging of the Helmholtz layer

$$j = j^{sc} + \left(C_{sc} \frac{d\phi_{sc}}{dt} + j_{ss}\right) = j^H + C_H \frac{d\phi_H}{dt} \tag{11}$$

$$j^H = k_3 p_2 \tag{12}$$

$$j^{sc} = I_0 - k_4 p_2 \tag{13}$$

For the sake of simplicity, in the following we consider only the ac component of all variables and mark them with a tilde.. If, in addition to a dc potential, a small-signal simusoidally varying potential perturbation with frequency $\omega/2\pi$ is applied across the cell, the amplitude of the resulting variation of the current density may be written as the complex quantity ($i = \sqrt{-1}$)

$$\tilde{j} = \tilde{j}^{sc} + (i\omega C_{sc} \tilde{\phi}_{sc} + \tilde{j}_{ss}) = \tilde{j}^H + i\omega C_H \tilde{\phi}_H \tag{14}$$

As stated above, it is assumed that an applied potential perturbation, $\tilde{U} = |U| \exp(i\omega t)$, across the interface results in a variation of the potential drop across both the semiconductor and the Helmholtz layer, where $|U|$ is the amplitude. In the presence of compensated electrolyte resistance, R_s, or if it is sufficiently small, this means (see Appendix)

$$\tilde{U} \approx \tilde{\phi} = \tilde{\phi}_{sc} + \tilde{\phi}_H \tag{15}$$

The electrochemical impedance $Z(\omega)$ is the inverse of the electrochemical admittance. The admittance $Y(\omega)$ itself is defined as the ratio

$$Y(\omega) = 1/Z(\omega) = \tilde{j}/\tilde{\phi} = \tilde{j}^H/\tilde{\phi} + i\omega C_H \tilde{\phi}_H/\tilde{\phi} \tag{16}$$

The derivation of $\tilde{\phi}_H/\tilde{\phi}$ and $Z(\omega)$ are given in the Appendix. The general impedance expressions are given by eqs 17 and 18 listed in Table 1 for the cases A and B, respectively. Equation 18 can be regarded as a special case for eq 17 as β equals zero.

In general, eq 17 or 18 predicts the appearance of two semicircles in the complex plane plot of Im(Z) vs Re(Z) as a function of frequency. The analysis is relatively straightforward if charge transfer and recombination occur on a longer time scale than the charging of the surface state capacitance. Under this condition, the contribution of surface state capacitance to the impedance response at low frequency may be negligible.

It can be seen from eq 17 or 18 that impedance measurements over a wide range of frequencies may give information about the interfacial capacitance $C = C_H C_{sc}/(C_H + C_{sc})$ and the rate constants k (neglecting R_s). As follows from these equations, the experimental EIS results allow one, in principle, to find the values of the kinetic parameters of the photoprocesses. At relatively low frequency it is possible to neglect $i\omega C$ in eq 17 or 18; thus the impedances of the second semicircle are described by eqs 19 and 20, respectively. In the low-frequency limit, the plot tends toward the real axis at the point $Z_{\omega \to 0}$. As the frequency increases, the imaginary component of the impedance passes through a maximum at a frequency ω^l_{max} before decreasing to intersect the real axis at Z_{high}. If the light intensity is selected appropriately, some limiting expressions can be easily derived from eqs 19 and 20. Two limiting cases of light intensity, i.e., strong and weak illumination, will be analyzed. For strong illumination, it is satisfied with $I_0 \gg C_H (k_3 + k_4)\kappa T/\beta q$, if $C_H = 4 \times 10^{-3}$ F cm^{-2}, $\beta = 0.5$, $(k_3 + k_4) = 3.15$, thus $I_0 \gg 6.48 \times 10^{-4}$ A cm^{-2}. On the contrary, for

TABLE 1: Summary of Characteristic Parameters of EIS for Cases A and B

parameters	case A (k_3 dependent on ϕ_H)	eq no.	case B (k_3 independent of ϕ_H)	eq no.
	General Case			
$Z(\omega)$	$R_s + \dfrac{C_H + C_{sc} + \dfrac{C_{ss}}{1+i\omega\tau_{ss}} + \dfrac{\alpha(q/\kappa T)k_4I_0 + \beta(q/\kappa T)k_3I_0}{(k_3+k_4)(k_3+k_4+i\omega)}}{C_H\left[i\omega\left(C_{sc}+\dfrac{C_{ss}}{1+i\omega\tau_{ss}}\right)+\dfrac{\alpha(q/\kappa T)k_4I_0(k_3+i\omega)}{(k_3+k_4)(k_3+k_4+i\omega)}\right]+\left(C_{sc}+\dfrac{C_{ss}}{1+i\omega\tau_{ss}}\right)\dfrac{\beta(q/\kappa T)k_3I_0(k_4+i\omega)}{(k_3+k_4)(k_3+k_4+i\omega)}+\dfrac{\alpha(q/\kappa T)k_4I_0\beta(q/\kappa T)k_3I_0}{(k_3+k_4)^2(k_3+k_4+i\omega)}}$	(17)[a]	$R_s + \dfrac{\left(C_H + C_{sc} + \dfrac{C_{ss}}{1+i\omega\tau_{ss}}\right) + \dfrac{\alpha(q/\kappa T)k_4I_0}{(k_3+k_4)(k_3+k_4+i\omega)}}{C_H\left[i\omega\left(C_{sc}+\dfrac{C_{ss}}{1+i\omega\tau_{ss}}\right)+\dfrac{\alpha(q/\kappa T)k_4I_0(k_3+i\omega)}{(k_3+k_4)(k_3+k_4+i\omega)}\right]}$	(18)
$Z(\omega)$ of the second semicircle	$\dfrac{1+\dfrac{\alpha(q/\kappa T)k_4I_0+\beta(q/\kappa T)k_3I_0}{(C_H+C_{sc})(k_3+k_4)(k_3+k_4+i\omega)}}{\dfrac{\alpha(q/\kappa T)k_3k_4I_0}{(C_H+C_{sc})(k_3+k_4)(k_3+k_4+i\omega)}\left(C_H+C_{sc}+\dfrac{\beta(q/\kappa T)I_0}{k_3+k_4}\right)+\dfrac{i\omega[\alpha(q/\kappa T)C_Hk_4I_0+\beta(q/\kappa T)C_{sc}k_3I_0]}{(C_H+C_{sc})(k_3+k_4)(k_3+k_4+i\omega)}}$	(19)	$\dfrac{1+\dfrac{\alpha(q/\kappa T)k_4I_0}{(C_H+C_{sc})(k_3+k_4)(k_3+k_4+i\omega)}}{\dfrac{\alpha(q/\kappa T)C_Hk_4I_0(k_3+i\omega)}{(C_H+C_{sc})(k_3+k_4)(k_3+k_4+i\omega)}}$	(20)
$Z_{\omega\to0}$	$\dfrac{1+\dfrac{\alpha(q/\kappa T)k_4I_0+\beta(q/\kappa T)k_3I_0}{(C_H+C_{sc})(k_3+k_4)^2}}{\dfrac{\alpha(q/\kappa T)k_3k_4I_0}{(C_H+C_{sc})(k_3+k_4)^2}\left(C_H+C_{sc}+\dfrac{\beta(q/\kappa T)I_0}{k_3+k_4}\right)}$	(21)	$\dfrac{1+\dfrac{\alpha(q/\kappa T)I_0k_4}{(C_H+C_{sc})(k_3+k_4)(k_3+k_4)}}{\dfrac{\alpha(q/\kappa T)C_Hk_3k_4I_0}{(C_H+C_{sc})(k_3+k_4)(k_3+k_4)}}$	(22)
ω^1_{max}	$k_3\left[1+\dfrac{C_{sc}}{C_H}+\dfrac{\beta qI_0}{\kappa TC_H(k_3+k_4)}\right]=k_3(1+C_{sc}/C_H)+\beta qj_{st}/(\kappa TC_H)$	(23)	k_3	(24)
Z_{high}	$(C_H+C_{sc})(k_3+k_4)/[\alpha(q/\kappa T)C_Hk_4I_0+\beta(q/\kappa T)C_{sc}k_3I_0]$	(25)	$(C_H+C_{sc})(k_3+k_4)\kappa T/(\alpha qC_Hk_4I_0)$	(26)
	Case I: Strong Light Intensity with $I_0 \gg C_H(k_3+k_4)\kappa T/\beta q$			
$Z(\omega)$ of the second semicircle	$\dfrac{\alpha(q/\kappa T)k_4I_0+\beta(q/\kappa T)k_3I_0}{\dfrac{\alpha(q/\kappa T)k_3k_4I_0\beta(q/\kappa T)I_0}{k_3+k_4}+i\omega\alpha(q/\kappa T)C_Hk_4I_0}$	(27)	$1/[C_H(k_3+i\omega)]$	(28)
$Z_{\omega\to0}$	$(\alpha k_4+\beta k_3)(k_3+k_4)q/(\kappa T\alpha\beta k_3k_4I_0)$	(29)	$1/(C_Hk_3)$	(30)
ω^1_{max}	$\omega^1_{max}=\dfrac{\beta(q/\kappa T)k_3I_0}{C_H(k_3+k_4)}=\dfrac{\beta q/\kappa TC_H}{j_{st}}$	(31)	k_3	(32)
Z_{high}	$(\alpha k_4I_0+\beta k_3I_0)/(i\omega C_H\alpha k_4I_0)$	(33)	$1/(i\omega C_H)$	(34)
	Case II: Weak Light Intensity with $I_0 \ll C_H(k_3+k_4)\kappa T/\beta q$			
$Z(\omega)$ of the second semicircle	$(C_H+C_{sc})(k_3+k_4)(k_3+k_4+i\omega)/[\alpha(q/\kappa T)k_3k_4I_0(C_H+C_{sc})+i\omega\alpha(q/\kappa T)C_Hk_4I_0]$	(35)	$(C_H+C_{sc})(k_3+k_4)(k_3+k_4+i\omega)/[\alpha(q/\kappa T)C_Hk_4I_0(k_3+i\omega)]$	(36)
$Z_{\omega\to0}$	$(k_3+k_4)^2/[\alpha(q/\kappa T)k_3k_4I_0]$	(37)	$(C_H+C_{sc})(k_3+k_4)^2/[\alpha(q/\kappa T)C_Hk_3k_4I_0]$	(38)
ω^1_{max}	$k_3(1+C_{sc}/C_H)$	(39)	k_3	(40)
Z_{high}	$(C_H+C_{sc})(k_3+k_4)\kappa T/(\alpha qC_Hk_4I_0)$	(41)	$(C_H+C_{sc})(k_3+k_4)\kappa T/(\alpha qC_Hk_4I_0)$	(42)

[a] Where $\tau_{ss} = R_{ss}C_{ss}$.

weak illumination, it is set as $I_0 \ll C_H(k_3 + k_4)\kappa T/\beta q$. This limitation can readily be obtained by controlling light source intensity. For each case, its corresponding characteristic parameters are listed in Table 1. (The process of calculating these parameters can be found in the Appendix.)

It can be seen from Table 1 that, under weak illumination, the differences between the $Z_{\omega\to 0}$ and Z_{high} that represent the arc size on the EIS plot are identical for cases A and B. Thus we cannot distinguish the two cases only by using this parameter. However, they may be distinguishable by the ω^l_{max} as shown by eqs 39 and 40, since ω^l_{max} should not depend on the applied potential for case B but do for case A. It is important to note that, under strong illumination, according to eq 31, C_H can be obtained by the slope of linear relationship between ω^l_{max} and steady-state photocurrent j_{st}. Thus, when C_{sc} and C_H are known, combining steady-state photocurrent measurements, according to eq 23, k_3 can be readily obtained by experimental EIS carried out at any given light intensity. Once k_3 is known, therefore, in principle, k_4 can be obtained by the ratio of $Z_{\omega\to 0}/Z_{high}$.

3. Experimental Section

The anatase TiO_2 photoelectrodes were prepared by a sol−gel technique described in ref 6. The exposed area of the TiO_2 film electrodes was 0.78 cm^2; the rest was covered with expoxy resin. Further details on the preparation procedures and photocatalyst characterization can be found elsewhere.[6]

All solutions were prepared using reagent grade chemicals. The indifferent electrolyte was always a 0.5 M Na_2SO_4 aqueous solution.

Electrochemical and photoelectrochemical measurements were carried out in a conventional three-electrode cell with a quartz window, closed from air, using a saturated calomel electrode (SCE) as the reference electrode and a platinum wire as the counter electrode. To keep the cell oxygen free, nitrogen was bubbled through the electrolyte prior to and between all measurements while it was blown over the solution during the measurements. All potentials were measured with respect to SCE in the text.

The cell potential was controlled by a model EG &G 273A potentiostat (Princeton Applied Research), which allows both current−potential and impedance measurements. The electrochemical impedance spectra were recorded in the potentiostatic mode, meaning that the dc potential is kept constant while an impedance spectrum is recorded. The interfacial capacitance as a function of the applied electrode potential (Mott−Schottky plot) was obtained at 10 kHz without illumination.

The amplitude of the sinusoidal wave was 10 mV, and the frequency range examined was 100 kHz to 0.01 Hz. The amplitude and phase of the resulting modulated EIS were measured with a PAR 5210 lock-in analyzer. For the PEC measurements, the electrode was illuminated with a UV light, which emitted from a 250 W lamp (type SVX 1450, Müller Electronik Optic, Germany). The incident light intensity was controlled by placing stainless steel mesh between the lamp and the cell. The data acquisition and processing were performed with a PC-type computer with specially designed software.

The photocatalytic degradation reactions of salicylic acid were performed in the above-described three-electrode system, either 150 or 5 cm^3 solutions were used. Other conditions were the same as for the experimental conditions of EIS. The salicylic acid concentration in the solution was estimated colorimetrically (752 spectrophotometer, Shanghai) according to the procedures described in ref 25.

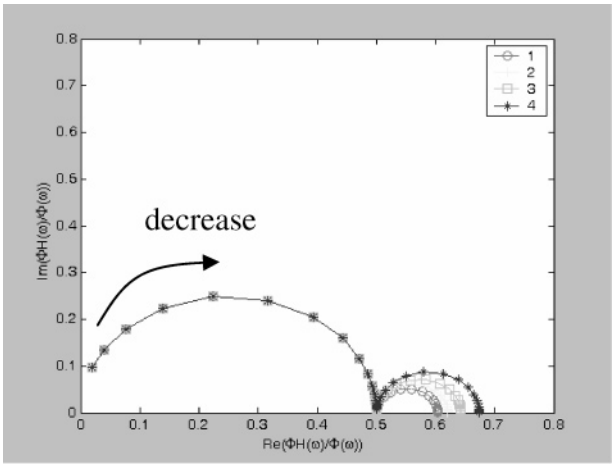

Figure 2. Plot of the imaginary part of $\tilde{\phi}_H/\tilde{\phi}$ as a function of the frequency from eq A20 with $C_H = 4 \times 10^{-3}$ F cm^{-2}, $C_{sc} = 4 \times 10^{-6}$ F cm^{-2}, $C_{ss} = 4 \times 10^{-3}$ F cm^{-2}, $I_0 = 6 \times 10^{-4}$ A cm^2, $k_3 = 0.15$, $\tau_{ss} = 1 \times 10^{-4}$ s, $\alpha = \beta = 0.5$, and (1) $k_4 = 5.0$, (2) $k_4 = 4.0$, (3) $k_4 = 3.0$, (4) $k_4 = 2.0$.

4. Results and Discussion

4.1. Theoretical Simulation Using the EIS Model. The diagnostic features of the calculated EIS responses should extend the range of application of the technique. The parameters of PEC decomposition of salicylic acid were used in the EIS expression simulations. The capacitance of the depletion layer, C_{sc}, is less than C_H and simply given by the Mott−Schottky relation. The C_H is assumed to be 4×10^{-3} F cm^{-2}. Under these conditions, some of the main features of the EIS signatures can thus be illustrated for different cases. First, the relationship between the harmonically varying potential drop $\tilde{\phi}_H$ and the modulation potential $\tilde{\phi}$ of the cell will be considered in more detail. Equation A20 in the Appendix gives such a relation. In Figure 2 the $\tilde{\phi}_H/\tilde{\phi}$ is plotted in the complex plane at different charge recombination rate constants for the case A. It shows that the distribution of $\tilde{\phi}$ over the Helmholtz layer depends on the frequency for each case. In the high-frequency domain, this distribution is insensitive to the k_4; however, it increases with decreasing k_4 in the relatively low-frequency range. This phenomenon is due to relaxation of charge of the surface state (an accumulation of trapped holes at the surface will result in an increase in the potential drop over the Helmholtz layer). In fact, if the measuring frequency is much higher than k_3 and k_4, the $\tilde{\phi}_H/\tilde{\phi}$ approaches to the high-frequency limit, given by$C_{sc}/(C_H + C_{sc})$. Since C_{sc} is comparable to C_H for highly doped TiO_2, this high-frequency limit is not zero. If the measuring frequency is much lower than k_3 and k_4, $\tilde{\phi}_H/\tilde{\phi}$ equals the low-frequency limit, given by

$$\frac{\alpha q k_4 I_0/\kappa T(k_3 + k_4) + (C_{sc} + C_{ss})(k_3 + k_4)}{\alpha q k_4 I_0/\kappa T(k_3 + k_4) + \beta q k_3 I_0/\kappa T(k_3 + k_4) + (C_H + C_{sc} + C_{ss})(k_3 + k_4)} \quad (43)$$

Clearly, it depends on the rate constant. In addition, the $\tilde{\phi}_H/\tilde{\phi}$ is also dependent on the light intensity as indicated in Figure 3. Particularly, at strong light intensity, the applied potential will almost drop across the Helmholtz layer, which will affect the charge-transfer rate as will be demonstrated later. A modulation of k_3 will, in turn, decrease the potential distribution over the Helmholtz layer as indicated in Figure 3. It is also found that the $\tilde{\phi}_H/\tilde{\phi}$ is less dependent on τ_{ss} unless its value is comparable to the rate constant (not shown here). In principle, due to the fact that $\tilde{\phi}_H/\tilde{\phi}$ depends on the measuring frequency,

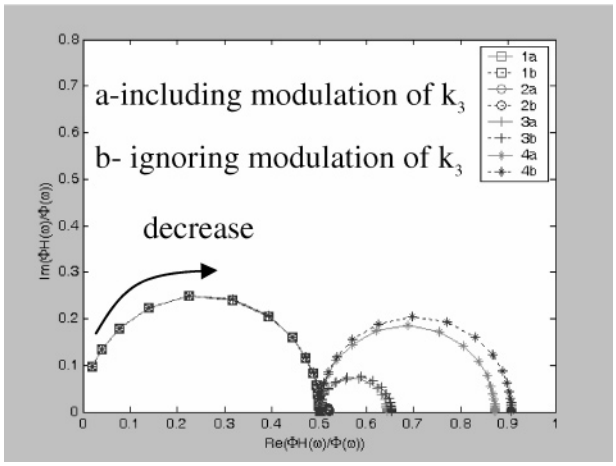

Figure 3. Plot of the imaginary part of $\tilde{\phi}_H/\tilde{\phi}$ as a function of the frequency from eq A20 with $k_4 = 3.0$, and (1) $I_0 = 6 \times 10^{-6}$ A cm^2, (2) $I_0 = 6 \times 10^{-5}$ A cm^2, (3) $I_0 = 6 \times 10^{-4}$ A cm^2, (4) $I_0 = 6 \times 10^{-3}$ A cm^2. Other parameters are given in Figure 2.

it is not possible to split the electrical impedance into depletion layer and the Hemholtz-layer components as shown by eq 17.

According to eq 17, some of the main features of the EIS responses are illustrated in Figures 4 and 5.

It can be seen from Figure 4 that when C_{ss} equals zero, two distinguishable semicircles in the Nyquist plot or two peaks in the Bode plot can be observed. As the C_{ss} increases, the peak in the Bode plot moves toward the low-frequency range while the two semicircles in the Nyquist plot gradually become indistinguishable. At the conditions where C_{ss} is larger than the Helmholtz capacitance, only one semicircle in the Nyquist plot and one peak in the Bode plot can be observed. Since C_H is in series with a parallel combination of C_{ss} and C_{sc}, from the theoretical EIS model one can conclude that the condition for surface states to influence the impedance response is that C_{ss} should be of comparable magnitude to C_{sc}. However, it has little influence on impedance response at low frequency (the second semicircle in the complex plane) for each case as indicated in Figure 4.

The time constant of charging of surface states, τ_{ss}, does also essentially not influence the second semicircle when it is smaller than the charge-transfer rate constant. With increase of k_3, the second arc size decreases (not shown here). Therefore, the arc diameter should give information about the charge recombination and transfer rate constants. In addition, the appearance of two distinguishable semicircles is found to depend on the light intensity as shown in Figure 5. At rather strong light intensity, it appears as two peaks in the Bode plot as indicated in Figure 5B. It is worth noting that, for case A, as predicted, the ω^l_{max} of the second semicircle depends on light intensity (also on k_4, thus on potential bias) but almost not for case B under relative high light intensity as indicated in Figure 5B.

4.2. Experimental EIS Display. A typical EIS response of illuminated TiO_2 electrode obtained at different potentials in the presence of salicylic acid is shown in Figure 6. In each case, only one arc and one peak can be observed on the Nynquist plot and on the Bode plot, respectively. That another capacitive arc is not observed here is probably due to that the time constant of the first circle is too small to be detected under the present frequency domain. Also, these results suggest that such a PEC degradation reaction appears to be a simple electrode process where the electrode potential is the only state variable.[25,31] These results allow one to derive kinetic parameters of the photoprocesses as will be demonstrated below.

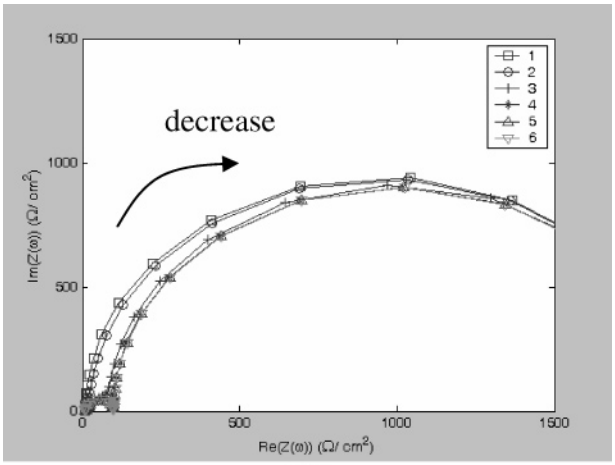

(A)

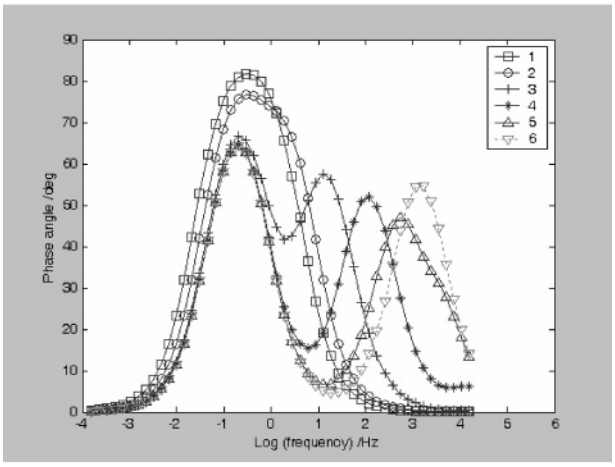

(B)

Figure 4. The EIS response calculated from eq 17. $C_H = 4 \times 10^{-3}$ F cm^{-2}, $C_{sc} = 4 \times 10^{-6}$ F cm^{-2}, $I_0 = 6 \times 10^{-4}$ A cm^2, $k_3 = 0.15$, $k_4 = 3.0$, $\tau_{ss} = 1 \times 10^{-4}$ s, $\alpha = \beta = 0.5$, $R_s = 10\ \Omega$, and (1) $C_{ss} = 4 \times 10^{-2}$ F cm^{-2}, (2) $C_{ss} = 4 \times 10^{-3}$ F cm^{-2}, (3) $C_{ss} = 4 \times 10^{-4}$ F cm^{-2}, (4) $C_{ss} = 4 \times 10^{-5}$ F cm^{-2}, (5) $C_{ss} = 4 \times 10^{-6}$ F cm^{-2}, (6) $C_{ss} = 0$ F cm^{-2}. (A) Nyquist plot; (B) Bode plot.

As predicted by the theoretical analysis or model simulation results, the ω^l_{max} increased with increasing the applied potential bias as indicated in Figure 6 while the arc diameter decreased, which is agreement with the previous reports.[23−27]

Figure 7 presents the EIS differences between those obtained in background electrolyte and with salicylate under UV illumination at various potentials. The EIS arcs observed with salicylate are smaller than those in the background solution at the same conditions. In addition, as can be seen from the inset in Figure 7, with salicylate the photocurrent is larger than those in the background solution, even a slightly negative photocurrent onset potential can be observed. These phenomena will be explained later.

We will first demonstrate whether the applied potential changes the charge-transfer rate constant k_3 (case A) or not (case B). For case B, according to eq 24, the ω^l_{max} should be independent of the applied potential. However, as stated above, it is found that the ω^l_{max} increased as the potential bias increased. Moreover, according to case B it predicts that ω^l_{max} is independent of the light intensity, but the ω^l_{max} increased substantially as the light intensity increased as indicated in Figure 8. These results indicate that the experimental EIS cannot be well explained by case B. Thus case A should be the fact.

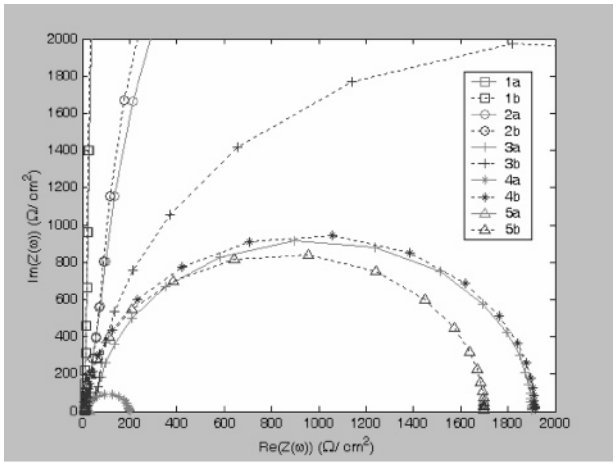

(A)

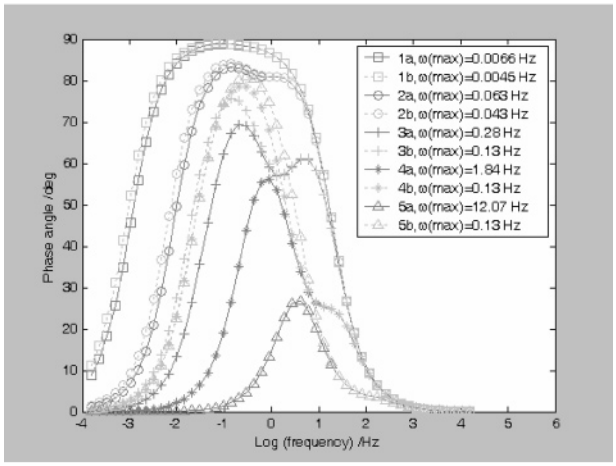

(B)

Figure 5. The EIS response calculated from eq 17 with $C_{ss} = 1 \times 10^{-3}$ F cm^{-2}, $\tau_{ss} = 10^{-4}$ s, $k_4 = 3.0$, and (1) $I_0 = 6 \times 10^{-6}$ A cm^2, (2) $I_0 = 6 \times 10^{-5}$ A cm^2, (3) $I_0 = 6 \times 10^{-4}$ A cm^2, (4) $I_0 = 6 \times 10^{-3}$ A cm^2, (5) $I_0 = 6 \times 10^{-2}$ A cm^2: (a) including modulation of k_3; (b) ignoring modulation of k_3. Other parameters are given in Figure 4. (A) Nyquist plot; (B) Bode plot. ω_{max} in part B represents characteristic angular frequency of the second semicircle (see text).

To further confirm this, for case A under strong light intensity, a good linear relationship is obtained between the ω^l_{max} and steady-state photocurrent j_{st} of the electrode (seen Figure 9, coefficient $\gamma^2 = 0.996$). This is in good agreement with the theoretical prediction as indicated by eq 31. Therefore, the above results indicate that a substantial fraction of the potential change appears across the Helmholtz layer (Fermi level pinning), which also changes the charge-transfer rate constant.

If $\beta = 0.5$, the slope of the straight line in Figure 9 gave $C_H = 4.3 \times 10^{-3}$ F cm^{-2}. When C_H is known, C_{sc} can be measured under dark at high frequency, and according to eq 23, k_3 can thus be obtained. Following this idea, the parameter k_3 derived from the EIS data under a typical photoelectrocatalytic degradation experiment is shown in Table 2. Obviously, increasing applied potential leads to an increase in the charge-transfer rate constant. It is also found that the magnitude of the rate constant is in good agreement with that of literature (at a potential of 0.6 V, $k_3 = 1.4$).[13] The fact that the rate constant k_3 increased as the potential bias increased is expected as indicated by eq 6, but the increase in k_3 (0.5 for a applied potential change of 0.15 V if $\beta = 0.5$) is smaller than the value expected (18.5 for a potential change of 0.15 V if $\beta = 0.5$). This indicates that most of the potential change appears across the depletion layer, which changes the charge recombination rate constant k_4.

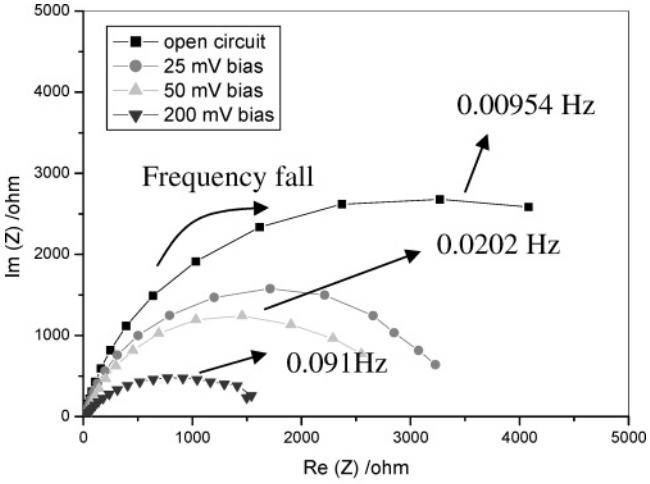

(A)

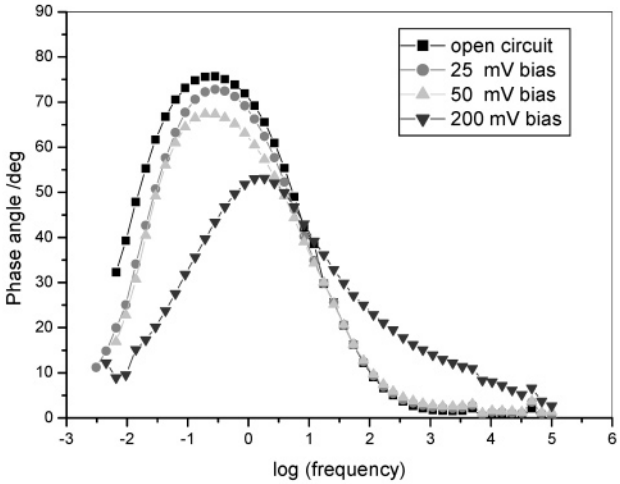

(B)

Figure 6. Effect of applied potential bias on the EIS plane display of the PEC reaction of 1 mM salicylic acid (pH = 4.0). The saturated photocurrent $j_{sat} = 0.22$ mA. (A) Nyquist plot; (B) Bode plot.

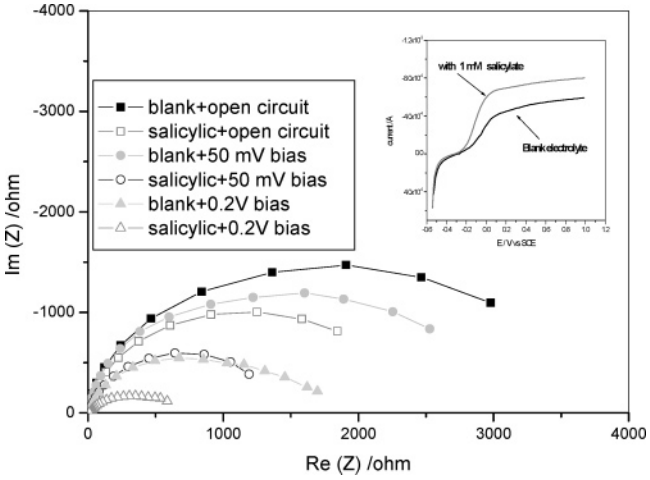

Figure 7. A Comparison of EIS in blank electrolyte and in 1 mM salicylic acid solutions (pH = 4.0). The inset shows the experimental current−potential curve under illumination. As can be seen with salicylate, the photocurrent is larger than those in the background solution, and also a little more negative photocurrent onset potential can be observed.

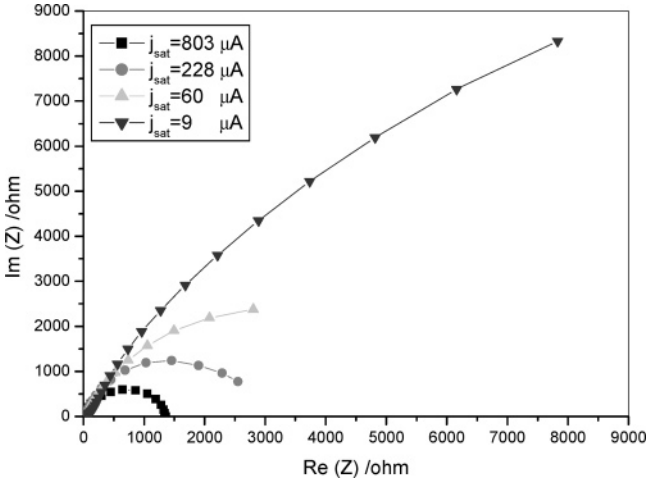

Figure 8. Effect of light intensity on the EIS plane display of the PEC reaction of 1 mM salicylic acid. Potential bias = 0.05 V. Other experimental conditions are the same as those given in Figure 6.

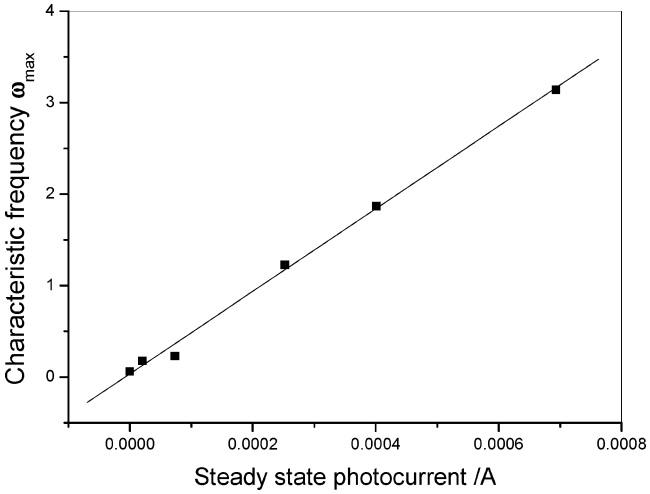

Figure 9. The plot of characteristic frequency ω^{l}_{max} vs the steady-state photocurrent j_{st} under strong light intensity illumination (j_{sat} = 3.5×10^{-3} A). Other experimental conditions are the same as those given in Figure 8.

TABLE 2: Potential Dependence of Charge Transfer Rate Constants (Saturation Photocurrent ~0.22 mA, 1 mM Salicylic Acid, pH = 4.0)

E/V vs open circuit	k_3/cm^4 s^{-1}	*E*/V vs open circuit	k_3/cm^4 s^{-1}
0.025	0.131	0.15	0.389
0.05	0.144	0.2	0.64
0.1	0.236		

Second, we will clarify the relevance of surface states. From a physical point of view, a surface state is an intraband gap electronic level that arises from incomplete coordination of the atoms present at the interface by other lattice atoms giving rise to dangling bonds or coordinative unsaturated sites.[32] Chemically, such surfaces states may be identified with titanium(IV) ions present at the TiO_2/solution interface that are partially coordinated to water molecules. These sites act as electron traps.[32] It is well documented that salicylic acid is strongly chemisorbed onto a TiO_2 surface, particularly in acid aqueous solutions, forming the inner-sphere titanium(IV)−salicylate surface complexes.[7,32−38] These surface complexes are considered to be the chemical counterparts of surface states.[36] Grätzel et al. have pointed out that as the water coordinated to Ti(IV) was replaced by the adsorbates, the trap depth of the surface state was expected to decrease, and if the lewis basicity of the ligand was strong enough, the electronic level of the surface state would be swept into the conduction band implying that its trapping action would vanish, suggesting the removal of surface states by complexation with the adsorbate.[32] This effect can also be demonstrated by impedance analysis as indicated below.

Analyses of the impedance due to surface states both in the dark and under illumination were conducted by using the approach reported by Searson and co-workers.[39,40] The measured impedance, *Z*, was interpreted on the basis of an equivalent circuit consisting of a resistance, R_s (due to the solution, contacts, and the leads), in series with a parallel combination of a frequency-dependent pseudocapacitance, C_p, and pseudoresistance R_p. We concentrate on C_p which is obtained from the real and imaginary parts of the measured impedance Re(*Z*) and Im(*Z*), respectively, using $C_p(E_{appl},\omega) = [\omega\ \mathrm{Im}(Z)(1 + D^2)]^{-1}$, in which *D* equals $[(\mathrm{Re}(Z) - R_s)/-\ \mathrm{Im}(Z)]$. The contributions from the interface states and/or recombination centers are obtained by subtracting the space-charge-layer capacitance C_{sc} from the total measured capacitance (C_{sc} was generally at least 1 order of magnitude smaller than the low-frequency capacitance maximum).

Figure 10 shows the parallel capacitance (C_p) under various conditions plotted against the applied potential. This provides a convenient method for distinguishing between the various interface states. [39] According Searson and co-worker's analysis, the low magnitude of the capacitance peak suggested low surface state density; the different position of the capacitance peak may involve diverse surface states.[39,40] In the dark, as shown in Figure 10A, the magnitude of the parallel capacitance in the presence of salicylate is lower than that of its absence, and also its position of the capacitance peak is different at the same frequency. These results further indicate that adsorption of salicylate decreased surface state density and even possibly gave rise to new surface states.

Next, the fact that under UV illumination the EIS arc observed with salicylate is smaller than that in the background solution at the same conditions can be explained as following. It has been proposed that holes from the valence band react with surface bound hydroxyl groups (and/or water and hydroxyl ions) that act also as effective mediators of water oxidation, generating surface radicals $Ti_SO^{\bullet}$.[1,28,33] These radicals would be responsible for (i) formation of surface peroxo species, $Ti_S-O-O-Ti_S$; (ii) surface recombination of h_{VB}^+ and e_{CB}^-, and (iii) electron exchange between the semiconductor and the species in solution. According to this model, compounds that can adsorb at the $Ti_SO^{\bullet}$ radical centers would undergo photooxidation more efficiently than water and OH^- ions, also reducing the number of recombination centers by diminishing the production of peroxo groups.[33] Regazzoni et al.[36] have considered that since the depth of surface hole traps must be determined by the lewis basicity of the ligands that complete the coordination sphere of the surface titanium ions, chemisorbed salicylate must be a deeper hole trap than bound OH^-, and that hole trapping by chemisorbed salicylate is expected to be kinetically less reversible; their results of differential diffuse reflectance spectrum of surface titanium(IV)−salicylate complexes favored the easier hole capture by chemisorbed salicylate. In addition, as Grätzel and co-workers[32] have pointed out that, apart from decreasing the trap depth of the surface state, replacing Ti(IV) coordinated water by salicylate may reduce the inner-sphere reorganization energy for electron transfer, increasing the nuclear factor and, consequently, increasing the interfacial electron transfer. Fur-

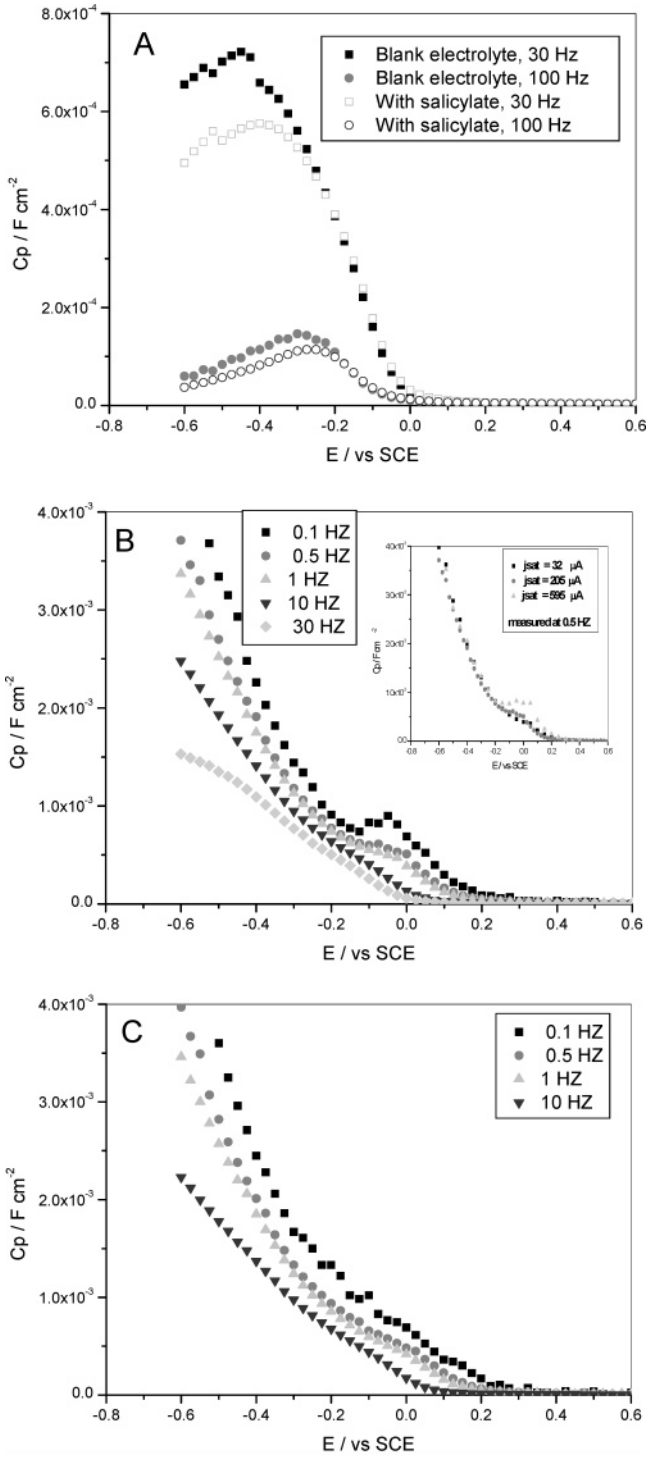

Figure 10. The measured parallel capacitance versus the applied potential at various frequencies in solutions of pH 4 for (A) dark, (B) illumination + blank electrolyte, and (C) illumination + 1 mM salicylate. The plateau photocurrent was 0.43 mA with 1 mM salicylate. These experiments were performed by stepping the potential from positive to negative potential, and the EIS response was measured at each potential. The magnitude amplitude was 5 mV (rms). The inset in B plot shows the dependence of the capacitance peak on illumination intensity in blank solutions.

thermore, using the electrochemical impedance technique, we observed that, under illumination, in blank electrolyte, the measured parallel capacitance exhibits a peak near 0.0 V that is not observed in the dark. The peak position, peak width, and peak height are dependent on frequency and light intensity as shown in Figure 10B. These features are characteristic of a surface recombination process.[39,40] However, when salicylate was added to the solution, the capacitance peak decreased or even vanished (see Figure 10C). It is also found that under strong enough light intensity, the magnitude of the peak was strongly dependent on the concentration of salicylic acid in the solution (not shown here). On the basis of Searson and co-worker's analysis,[39,40] from these results, one can conclude that addition of salicylate in the solution quenched those surface states produced under illumination. Therefore, from the above discussion it follows that in our case addition of salicylate results not merely in a reduction of the rate of surface recombination but in virtual enhancement of the process of charge transfer.

TABLE 3: Results for Photoelectrochemical Degradation of 1 mM Salicylic Acid Solutions after 40 min of Irradiation of a TiO_2 Electrode Polarized at Different Potentials[a]

potential/V vs open circuit	passed charge/C	degraded, %
0.05	0.085	~0[b]
0.1	0.29	~0[b]
0.2	1.62	6.9
1.0	5.18	25.1
0.1[c]	1.35	7.3

[a] 5 cm^3 solutions, other experimental conditions same as those in Figure 6. [b] No detectable salicylate degradation. [c] Illumination time: 180 min.

In general terms, the efficiency of the photocatalytic process is determined by the competition between the hole/electron recombination and the interfacial charge transfer to the electron donor/electron acceptor species. In turn, the actual rate of charge-transfer reactions is affected by the extent and strength of reactant adsorption on the TiO_2 surface.[1,37] In particular, strongly adsorbed organic species (either primary reactants or intermediates) may also cause inhibition of the photocatalytic degradation process at TiO_2. Such behavior has been reported in the case of salicylate[35,38] and 3-chloro-4-hydroxybenzoic acid.[41] Calvo et al.[38] have found the accumulation of intermediates and/or byproducts formed in anaerobic atmosphere were more evident for the pronounced concentrated salicylate solution during photoelectrocatalytic reaction. Therefore, it is necessary to examine if there was photodegradation of salicylate under the present experimental conditions of EIS, which might clarity the influence of partially oxidized intermediates on the EIS analysis.

When the experiments of photoelectrochemical oxidation of salicylate were conducted under the experimental conditions of EIS (solution volume 150 cm^3), i.e., the applied bias potential changing from 50 to 300mV (vs open circuit), illuminating for 40 min at each potential tested (a time longer than that needed for the EIS tests), unfortunately, in all cases no distinguishable difference of salicylate concentration before and after irradiation could be found by our analysis method (detection limits, 5×10^{-7} M). So we reduced the solutions to 5 cm^3, and the results obtained for the photodegradation are listed in Table 3. Again, in the cases of low applied bias potential, the degraded salicylate was too low to be detectable. However, either under high bias potential or at low potential but with longer illumination time, the photodegradation rate proceeded at an appreciable rate as shown in Table 3. Calvo[7,38] and Mandelbaum et al.[35] have reported similar results. Such a low rate is not surprising, considering the fact that complete mineralization to CO_2 involves the transfer of 28 holes in the absence of oxidants or homogeneous reactions and that the participation of photogenerated holes in parallel process, such as cleavage of water or photocorrosion, can hardly be precluded.[38]

Moreover, it has been stated that during PEC oxidation of salicylate partially oxidized intermediates can remain adsorbed

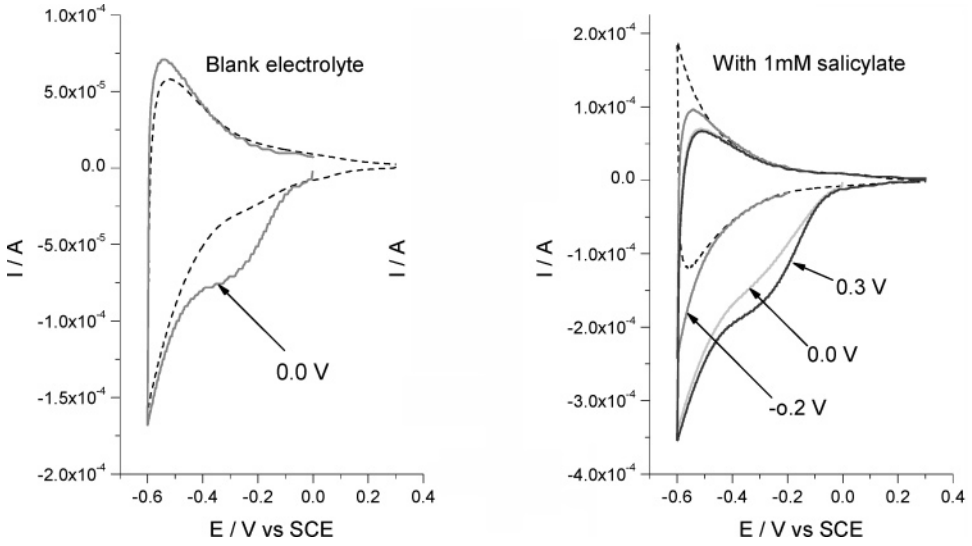

Figure 11. First cycle voltammograms run before (- - -) and after (—) 30 min of irradiation of salycilate or blank solutions in the presence of TiO_2 electrode biased at the indicated potentials (vs SCE) in the figure. Second and subsequent cycles after irradiation are nearly coincident with that recorded before irradiations.

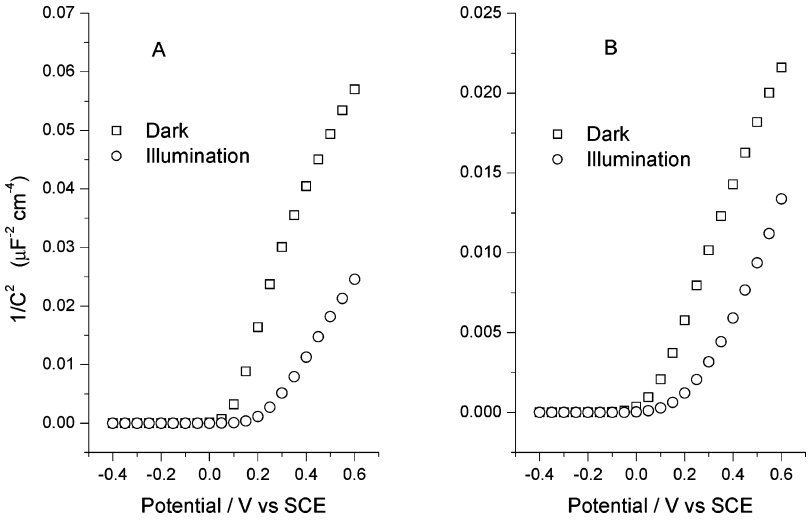

Figure 12. $C^{-2}-V$ diagram of the TiO_2 electrode in the dark (squares) and under illumination (circles) without (A) and with (B) 1 mM salicylic acid (pH = 4.0) in water. The saturated photocurrent with salicylate j_{sat} = 0.22 mA. These experiments were performed by applying the starting potential for 1 min and then performing a potential scan from positive to negative potential with a potential step of 50 mV and an equilibrium time of 10 s at each potential. The frequency was 10 Hz.

on the electrode surface, especially at sufficiently high substrate concentration, producing surface contamination,[38,42] which might change the EIS results. A series of experiments, similar to the reports of Calvo et al,[7,38] were conducted to check this. Briefly, the electrodes were illuminated at a fixed anodic potential for 30 min, and once the irradiation was stopped, a potential sweep from the applied potential to −0.6 V vs SCE in the dark was run to detect the reduction of fairly stable oxidized species formed on the electrode surface under illumination. Figure 11 shows that there is a considerable cathodic charge in the case of a high biased potential, in the voltammogram run after irradiation that is due to the presence of partially oxidized intermediates and/or byproducts on the surface;[7,38] note that the cathodic peak in the background electrolyte after irradiation is usually attributed to the photogenerated peroxo species, like hydrogen peroxide.[43] However, the accumulation of such species under illumination was not evident at low applied bias potential, which indicates their influence on the EIS analysis may be negligible. In fact, it was found that there was no evident difference in EIS results derived at low biased potential without and with illumination for 40 min before test even under the strongest light intensity used in the present experiments (not shown here). Under considerable salicylate concentration and high anodic bias, it was found[42] that even condensation reactions between radicals occurred leading to the growth of polymers on the surface that poisoned the active sites of the electrode. This is not the case in most of our experiments; thus we need not consider such a process in the EIS analysis.

Further remarks are presented for the energy band model that serves as a starting point for the calculation of the EIS model. The existence and possible role of surface states at n-type SEI have been pointed by various authors in electrochemical, photocurrent, and electroluminescence measurements.[12g,15−18] Unfortunately, it is very difficult to obtain direct experimental information about surface states.[12a] Figure 12 presents the effect of illumination on the capacitance of the electrode with and without salicylate, which is shown in a conventional Mott−Schottky diagram. It is obvious that a UV illumination caused the capacitance response in the Mott−Schottky plot to shift in the anodic direction and the capacitance to increase. Hagfeldt et al.[12h] have reported a similar phenomenon for the mesoporous TiO_2 electrode both in the supporting electrolyte and in aqueous

solutions of ethanol. We have also found (not shown here) that the photoeffect was sensitive to the nature of the ambient and light intensity as reported by Hagfeldt et al., confirming that the states involved in the capacitance charging of the TiO_2 film are at the surface and not in the interior of the particles.[12h] The origin of this effect has been explained by trapping of photogenerated holes in surface states, leading to a change of the band position.[12h,14,15] Such an unpinning of the energy bands was further confirmed by a dye-sensitization experiment.[12h] Liao and Walkeck[12i] have also demonstrated the presence of interfacial electronic states at the single crystalline TiO_2 electrode by photocapacitance spectroscopy, particularly where the adsorbate on the electrode is treated as a surface state. In summary, these results indicate that surface states take a role in the process of the hole transport in the present system. Besides this, during the initial stage of photocatalysis or PEC oxidation of organic compounds, although the nature of the interfacial hole transfer mechanism is, in some cases, the object of controversy, mainly because of the lack of experimental techniques able to give an unambiguous response, most authors found that photooxidation occurring indirectly via valence holes trapped at either surface-bound or interfacial OH radicals is the rule.[1,13,27,28] Surface states are commonly classified as either communicating with the semiconductor or with the contact electrolyte,[15,44] but the concept of the surface state is still poorly defined in the case of a boundary between two phases. In practice, there may be an interphase region with properties differing from those of the bulk, and atoms or ions may move across the phase boundary to form what could be termed "near surface states".[44] In this sense, the above-mentioned OH radicals may be regarded as photogenerating surface states.

The electron tunneling process must take place between states of equal energy.[12a,g] For the present system, because the equilibrium redox level of the R/R^+ couple is located considerably above the top of the valence band at the surface, the probability of direct hole transfer to salicylate dissolved in solution should be very low (process 1 in Figure 1). Conversely, the interfacial hole transfer between the filled electronic state in the ground state of salicylic acid molecule and the OH radical may be more efficient than that between the salicylic acid molecule and the hole in the valence band, because the energy difference of the former is smaller than that of the later. Of course, salicylate is specifically adsorbed, where a hole trapping is possible, but as stated above, the specially adsorbed species are assumed to be surface states. In this case, the hole transfer may occur through the chemisorbed species (surface states) to the physisorbed species in the interface region. The detail of the mechanism needs to be further demonstrated, which should require an addition experimental technique, although the experimental EIS results can be explained by the present mechanistic model. In addition, to further check the present mathematic EIS model, we have also attempted to simulate the experimental EIS results by eq 17 or 18, but it failed mainly due to too many variables to be fitted.

Finally, the above equations were derived for the simplest case of surface recombination occurring on a single type of surface state along with charge transfer to the solution. However, in some cases this mechanism can be complicated by follow-up electrochemical reaction diffusion of reacting species or photocurrent relaxation occurring at several types of surface states. However, from the above discussion it is ascertained that the simple analysis is applicable to complicated systems to some extent, although the information may be phenomenologically, qualitative rather than completely quantitative.

4.3. Correspondence to Impedance Expressions Found in the Literature. Up until now, we have made a mathematical calculation of the EIS of illuminated TiO_2 electrode processes involving charge transfer and recombination through surface states. Other impedance expressions describing transfer at illuminated semiconductor electrodes have been published previously.[20,27] It is instructive to compare these results with the impedance obtained here.

More than 10 years ago, Ponomarev and Peter proposed an impedance expression for photoelectrochemical hydrogen evolution at the illuminated p-InP/electrolyte interface to derive the rate constants of charge transfer and recombination.[20] As most of the previous models suggested, they also neglected the effect of the potential drop across the Helmholtz layer (which amounts to an infinite Helmholtz-layer capacitance) on the rate constants of charge transfer. Using the notation adopted in the present paper, the impedance expression obtained by them equals eq 18 when the surface state capacitance here and k_1 there equal zero. This model, however, cannot well explain the present experimental results as stated above.

More recently, Liu et al.[27] published a study on the impedance of OH radical mediated electron transfer at TiO_2/electrolyte junctions. In that work, the variation of the potential drops across the Helmholtz layer alone (though not stated clearly but actually as derived the impedance expression). This treatment is not popular, because for moderate or even highly doped semiconductor electrodes, the capacitance of the semiconductor side of the interface is supposed to be smaller than that of the Helmholtz layer.[15,22,23] As has been stated in section 4.1, such a case of complete Fermi level pinning only can be encountered if the light intensity is strong enough. In addition, their experimental results showed that there were two capacitive arcs/semicircles under a high electrical bias applied (higher than 200 mV vs SCE, see their Figure 7) and that there was only one capacitive arc/semicircle under a low bias (lower than 200 mV vs SCE). We have also found a similar phenomenon, i.e., as shown in Figures 13A, 6, and 7. Under a low bias (below 200 mV vs SCE) only one capacitive arc and only one peak appear on the EIS Nynquist plot and on the Bode plot, respectively, while under high bias potentials two peaks exhibit clearly on the Bode plot and also there are two capacitive arcs on the complex plot though the one at high frequency is covered by the other on the coordinate scale used. The two peaks on the Bode plot are more evident and the position of the one at high frequency shifts toward low frequency as the applied bias potentials increase. Liu et al.[27] concluded that of the two arcs on the EIS plane display, the first one represented the charger transfer step and the second one (under a low frequency) represented the adsorption step. However, this explanation cannot support our experimental EIS results as demonstrated below.

As shown in Figure 13B, under high applied potentials, even in the dark where no photoelectrochemical reactions existed, curves almost identical with those obtained with illumination can be observed at a high frequency, indicating it does not represent the charge transfer step. On the contrary, the one at low frequency changes with illumination, which should reflect the charge transfer step. In fact, by appropriately changing the surface area and thickness of electrode alone, two peaks/arcs are always observed both at high and low bias potential as shown in Figure 13C, further indicating the first arc at high frequency does not represent a charge-transfer step and hence the second one does not represent the adsorption step. As we know, a frequency dependence of Mott−Schottky is usually observed, which is often attributed to the surface state capacitance charging

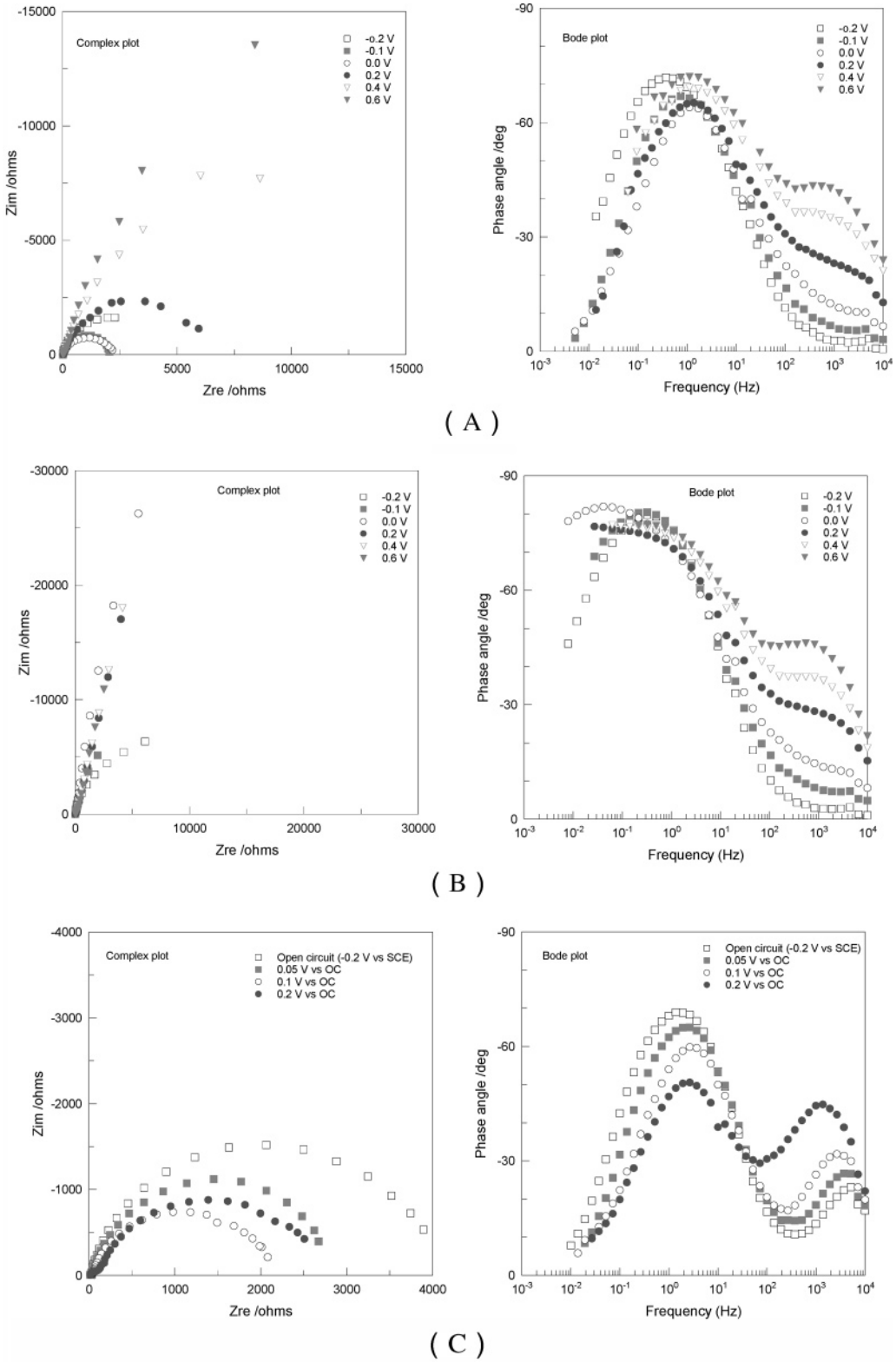

Figure 13. Effect of applied potential (vs SCE) on the EIS plane display of TiO_2 electrode in 1 mM salicylic acid aqueous solutions (pH = 4.0) with (A) and without (B) illumination. The saturated photocurrent $j_{sat} = 0.17$ mA. (C) EIS derived with TiO_2 electrode of 2 cm^2 and thicker film to demonstrate two peaks/arcs displaying even at low bias potential; $j_{sat} = 0.17$ mA, other experimental conditions are the same as those given in Figure 13A.

of the electrode.[15−18] When the applied anodic potentials increase, the Fermi level and C_{sc} decrease, C_{ss} may be comparable to C_{sc}, and the time constant at the semiconductor side of the interface increases; thus as predicted from the eq 17 and simulation results in section 4.1, two distinguishable peaks on the Bode plot or capacitive arcs on the complex plane plot may appear. On the basis of the above results, we argue that the arc/peak at high-frequency here is attributed to combined space charge/surface state/oxide film capacitances and associated resistances other than a charge-transfer step, while the one at a low frequency is attributed to the charge-transfer step but not the adsorption step.

A discussion of reports of Liu et al. and a detailed comparison with the present results are difficult, due to limited experimental

EIS results in that work, e.g., no Bode plot and the results in the dark. However, some notes may be presented: (i) most studies found that photocurrents are not limited by mass transfer,[8,13] as the solvent, water, which is present at a concentration of ca. 55 M, is able to be oxidized—a process difficult to compete with, so the adsorption-dominated reaction should be infrequent; (ii) EIS can only be used to obtain charge-transfer rate constants near the photocurrent onset region[15] as is the case here, if it is carried out at the approaching photocurrent saturation region, a distorted impedance arc or straight line similar to diffusion impedance may be observed as can be seen from Figure 13; (iii) since in the work of Liu et al.[27] the applied potentials are rather high (relative to SCE not open circuit, see their Figures 7 and 8), it might produce many adsorbable intermediates on the electrode surface (see Figure 11) that might result in surface contamination. Such behavior may cause the fluctuation of surface active sites of the electrode, thus introducing a new state variable or time constant; and (iv) they used poly(vinyl alcohol) (PVA) as a binder to immobilize TiO_2 on conducting substrate; however, PVA is also a sacrificial electron donor.[45] Likewise, its partially oxidized intermediates on the surface may hinder the PEC reactions, causing complexity in the EIS analysis.

Finally, an equivalent circuit with two capacitors and two resistors has been proposed by Schefold[23] to explain the process occurring at the illuminated lowly doped semiconductor. However, the equivalent circuit approach seems to us to be unsatisfactory since the physical meaning of the element is obscure.[20] In addition, an equivalent circuit is never a unique representation of an impedance expression.[30]

5. Summary

The electrochemical impedance mathematical model of TiO_2 photoelectrocatalytic reactions involving charge transfer and recombination through surface states was developed. The model was used to study the kinetics of PEC decomposition of salicylic acid. The model simulation results show that the appearance of two distinguishable semicircles in the EIS response depends on surface state capacitance and light intensity. The experimental results demonstrated that only one arc and one peak could be observed on the Nynquist plot and on the Bode plot under low bias potentials, respectively, which represents the charge transfer step. The charging of surface states does essentially not influence impedance responses at low frequency, which allows one to derive kinetic parameters of the photoprocesses directly. The model provides a way to obtain the rate constants for the photoelectrochemical reactions of surface states mediating charge transfer and recombination. The applied potential changed not only the recombination rate constant but also the charge-transfer rate constant. The experimental EIS results on PEC degradation reactions can be explained by the present model satisfactorily. It was demonstrated that EIS is a powerful tool for studying the kinetics of PEC decomposition of organic pollutants on TiO_2 electrodes.

Acknowledgment. The project was supported by the National Science Foundation Council of China (NSFC, Grant No. 20107006 and 20373062).

Appendix. Derivation of the EIS and Parameters in the Table 1

Under steady-state, solution of eqs 7, 8, and 12 gives the steady-state concentration of the respective parameters, ${p_1}^0$, ${p_2}^0$, and j_{st}

$$\frac{dp_1}{dt} = 0$$

$${p_1}^0 = I_0/k_2 \tag{A1}$$

$$\frac{dp_2}{dt} = 0$$

$${p_2}^0 = k_2{p_1}^0/(k_3 + k_4) = I_0/(k_3 + k_4) \tag{A2}$$

$$\frac{d\phi_H}{dt} = 0$$

$$j_{st} = k_3{p_2}^0 = k_3I_0/(k_3 + k_4) \tag{A3}$$

The potential of the semiconductor electrode with respect to the reference is

$$U - U_{Ref} = \phi_{sc} + \phi_H + R_sj - U_{Ref} = \phi + R_sj - U_{Ref} \tag{A4}$$

where R_s is the uncompensated electrolyte resistance (usually $\approx$10 Ω) and U_{Ref} is the potential of the reference electrode.

In impedance measurements, a small harmonic perturbation, $\tilde{U} = |U| \exp(i\omega t)$, is superimposed on the steady-state applied potential U, where $|U|$ is the amplitude. The system is assumed to behave in accordance with linear systems theory which requires stability, causality, and linearity.[31]By use of a small perturbation, the modulated parameters can be approximated by the first terms of their respective Taylor expansions. In the following, we will denote all modulated quantities with a tilde.

Since U_{Ref} is a constant, it follows from eq A4 that

$$\tilde{U} = \tilde{\phi} + R_s\tilde{j} \tag{A5}$$

If R_s is sufficiently small, then $\tilde{U} \approx \tilde{\phi}$.

The time-dependent perturbation of the recombination rate constant and charge-transfer rate constant is related to the potential drop across the depletion layer and Helmholtz layer, respectively. Following from eqs 5 and 6, we have

$$\tilde{k}_4 = (-\alpha q/\kappa T)k_4^\circ \exp\left(\frac{-\alpha q\phi_{sc}}{\kappa T}\right)\tilde{\phi}_{sc} = (-\alpha q/\kappa T)k_4\tilde{\phi}_{sc} = Ak_4(\tilde{\phi} - \tilde{\phi}_H) \tag{A6}$$

$$\tilde{k}_3 = (\beta q/\kappa T)k_3^\circ \exp\left(\frac{\beta q\phi_H}{\kappa T}\right)\tilde{\phi}_H = Bk_3\tilde{\phi}_H \tag{A7}$$

where $A = (-\alpha q/\kappa T)$ and $B = (\beta q/\kappa T)$.

Since I_0 is assumed to be independent of the applied potential, according to eq 7, the time dependent on the surface hole, $\tilde{p}_1$, is given by

$$\tilde{p}_1 = 0 \tag{A8}$$

Using eq 8, we can write that

$$\frac{d\tilde{p}_2}{dt} = i\omega\tilde{p}_2 = k_2\tilde{p}_1 - (\tilde{k}_3 p_2^{\,0} + k_3\tilde{p}_2) - (\tilde{k}_4 p_2^{\,0} + k_4\tilde{p}_2) \tag{A9}$$

Substitution of eqs A6−A8 into eq A9 yields after rearrangement

$$\tilde{p}_2 = -\frac{(\tilde{k}_3 + \tilde{k}_4)p_2^{\,0}}{(k_3 + k_4 + i\omega)} = \frac{p_2^{\,0}[-Bk_3\tilde{\phi}_H - Ak_4(\tilde{\phi} - \tilde{\phi}_H)]}{(k_3 + k_4 + i\omega)} \tag{A10}$$

Similarly, following from eqs 9 and 10, respectively, we have

$$\tilde{j}_{ss} = i\omega C_{ss}\tilde{\phi}_{ss} \tag{A11}$$

$$\tilde{j}_{ss}R_{ss} + \tilde{\phi}_{ss} = \tilde{\phi}_{sc} = \tilde{\phi} - \tilde{\phi}_H \tag{A12}$$

Eliminating $\tilde{\phi}_{ss}$ of eqs A11 and A12, we get

$$\tilde{j}_{ss} = \frac{i\omega C_{ss}(\tilde{\phi} - \tilde{\phi}_H)}{1 + i\omega\tau_{ss}} \tag{A13}$$

where $\tau_{ss} = R_{ss}C_{ss}$.

Using eqs 11−13, the ac component of the external photocurrent, $\tilde{j}$, can be written as

$$\tilde{j} = \tilde{j}^H + i\omega C_H\tilde{\phi}_H = \tilde{k}_3 p_2^{\,0} + k_3\tilde{p}_2 + i\omega C_H\tilde{\phi}_H \tag{A14}$$

$$\tilde{j} = \tilde{j}^{sc} + i\omega C_{sc}\tilde{\phi}_{sc} + \tilde{j}_{ss} = 0 - \tilde{k}_4 p_2^{\,0} - k_4\tilde{p}_2 + i\omega C_{sc}(\tilde{\phi} - \tilde{\phi}_H) + \tilde{j}_{ss} \tag{A15}$$

Substituting eqs A7 and A10 into eq A14, we get

$$\tilde{j} = Bk_3 p_2^{\,0}\tilde{\phi}_H + \frac{k_3 p_2^{\,0}[-Bk_3\tilde{\phi}_H - Ak_4(\tilde{\phi} - \tilde{\phi}_H)]}{(k_3 + k_4 + i\omega)} + i\omega C_H\tilde{\phi}_H \tag{A16}$$

Substituting eqs A6, A10, and A13 into eq A15, we obtain

$$\tilde{j} = -Ak_4 p_2^{\,0}(\tilde{\phi} - \tilde{\phi}_H) - \frac{k_4 p_2^{\,0}[-Bk_3\tilde{\phi}_H - Ak_4(\tilde{\phi} - \tilde{\phi}_H)]}{(k_3 + k_4 + i\omega)} + i\omega C_{sc}(\tilde{\phi} - \tilde{\phi}_H) + \frac{i\omega C_{ss}(\tilde{\phi} - \tilde{\phi}_H)}{1 + i\omega\tau_{ss}} \tag{A17}$$

As stated above, the admittance $Y(\omega)$ is calculated by dividing the modulated current by the modulated applied potential. Using eqs A16 and A17, respectively, we can get

$$Y(\omega) = \frac{\tilde{j}}{\tilde{\phi}} = Bk_3 p_2^{\,0}a + \frac{k_3 p_2^{\,0}[-Bk_3 a - Ak_4(1-a)]}{(k_3 + k_4 + i\omega)} + i\omega C_H a \tag{A18}$$

$$Y(\omega) = \frac{\tilde{j}}{\tilde{\phi}} = -Ak_4 p_2^{\,0}(1-a) - \frac{k_4 p_2^{\,0}[-Bk_3 a - Ak_4(1-a)]}{(k_3 + k_4 + i\omega)} + i\omega C_{sc}(1-a) + \frac{i\omega C_{ss}(1-a)}{1 + i\omega\tau_{ss}} \tag{A19}$$

where $a = \tilde{\phi}_H/\tilde{\phi}$.

Combination of eqs A18 and A19 yields after substitution for the p_2° [eq A2] and rearrangement

$$a = \tilde{\phi}_H/\tilde{\phi} = \frac{C_{sc} + C_{ss}/(1 + i\omega\tau_{ss}) + \alpha(q/\kappa T)k_4 I_0/(k_3 + k_4)(k_3 + k_4 + i\omega)}{C_H + C_{sc} + C_{ss}/(1 + i\omega\tau_{ss}) + \alpha(q/\kappa T)k_4 I_0/(k_3 + k_4)(k_3 + k_4 + i\omega) + \beta(q/\kappa T)k_3 I_0/(k_3 + k_4)(k_3 + k_4 + i\omega)} \quad \text{(A20)}$$

Substituting eq A20 into eq A18, gives the admittance expression for case A

$$Y(\omega) = \frac{C_H\left[i\omega\left(C_{sc} + \frac{C_{ss}}{1 + i\omega\tau_{ss}}\right) - \frac{Ak_4 p_2{}^0(k_3 + i\omega)}{(k_3 + k_4 + i\omega)}\right] + \left(C_{sc} + \frac{C_{ss}}{1 + i\omega\tau_{ss}}\right)\frac{Bk_3 p_2{}^0(k_4 + i\omega)}{(k_3 + k_4 + i\omega)} - \frac{Ak_4 p_2{}^0 Bk_3 p_2{}^0}{(k_3 + k_4 + i\omega)}}{C_H + C_{sc} + \frac{C_{ss}}{1 + i\omega\tau_{ss}} + \frac{Bk_3 p_2{}^0 - Ak_4 p_2{}^0}{(k_3 + k_4 + i\omega)}} \quad \text{(A21)}$$

Thus, the impedance, $Z(\omega) = 1/Y(\omega)$, is obtained and given by eq 17 listed in Table 1 after substitution for the $p_2{}^0$ (eq A2) and addition of the R_s.

Similarity, for case B, where k_3 is time independent, i.e., $\tilde{k}_3 = 0$, the impedance expression here is given by eq 18 listed in Table 1, and for this case, when neglecting jR_s potential drop, the $\tilde{\phi}_H/\tilde{\phi}$ is given by

$$\tilde{\phi}_H/\tilde{\phi} = \frac{C_{sc} + C_{ss}/(1 + i\omega\tau_{ss}) + \alpha(q/\kappa T)k_4 I_0/(k_3 + k_4)(k_3 + k_4 + i\omega)}{C_H + C_{sc} + C_{ss}/(1 + i\omega\tau_{ss}) + \alpha(q/\kappa T)k_4 I_0/(k_3 + k_4)(k_3 + k_4 + i\omega)} \quad \text{(A22)}$$

Below is presented how to obtain the other parameters listed in Table 1 using case A as an example. As stated above, at relatively low frequency it is possible to neglect the impedance response resulting from the interface charging/discharging ($i\omega C$); thus the remaining impedance of eq 17, which corresponds to the second semicircle, is described by

$$Z_{sec}(\omega) = \frac{1 + \frac{\alpha(q/\kappa T)k_4 I_0 + \beta(q/\kappa T)k_3 I_0}{(C_H + C_{sc})(k_3 + k_4)(k_3 + k_4 + i\omega)}}{\frac{(q/\kappa T)k_3 k_4 I_0}{(C_H + C_{sc})(k_3 + k_4)(k_3 + k_4 + i\omega)}\left(\alpha C_H + \beta C_{sc} + \frac{\alpha\beta(q/\kappa T)I_0}{k_3 + k_4}\right) + \frac{i\omega[\alpha(q/\kappa T)C_H k_4 I_0 + \beta(q/\kappa T)C_{sc}k_3 I_0]}{(C_H + C_{sc})(k_3 + k_4)(k_3 + k_4 + i\omega)}} \quad \text{(A23)}$$

It is reasonable to assume that α is of the same order of magnitude as β($\alpha \approx \beta$), thus eq A23 becomes eq 19. In the low-frequency limit ($\omega \rightarrow 0$), eq 19 reduces to eq 21, while at rather high frequency ($\omega \gg (k_3 + k_4)$), eq 19 becomes eq 25.

The characteristic frequency ω_{max}^{l} of eq A23 is

$$\omega_{max}^{l} = \frac{k_3[\alpha C_H k_4 + \beta C_{sc}k_4 + (\alpha\beta q/\kappa T)k_4 I_0/(k_3 + k_4)]}{(\alpha C_H k_4 + \beta C_{sc}k_3)} \quad \text{(A24)}$$

Considering that C_H is usually larger than C_{sc}, $\alpha \approx \beta$, and that $k_4 \gg k_3$, thus $\alpha C_H k_4 \gg \beta C_{sc}k_3$, therefore eq A24 reduces to eq 23.

Under strong enough light intensity where $I_0 \gg C_H(k_3 + k_4)\kappa T/\beta q$, eq 23 reduces to eq 31, while if $I_0 \ll C_H(k_3 + k_4)\kappa T/\beta q$, it becomes eq 39.

The other parameters for the two limiting case of light intensity can be easily obtained starting from their corresponding ones for the general case listed in Table 1.

Nomenclature

α = ideality factor of the junction
β = transfer coefficient
C = capacitance of interfacial layer, F cm^{-2}
C_H = capacitance of Helmholtz layer, F cm^{-2}
C_{sc} = capacitance of depletion layer, F cm^{-2}
C_{ss} = capacitance of surface state, F cm^{-2}
E_F = energy of surface state
E_s = Fermi level of semiconductor
F = Faradaic constant, 9.65 $\times$ 10^4 C mol^{-1}
f = frequency, Hz
h^+ = photogenerated hole
I_0 = flux of holes toward the surface, A cm^{-2}
$i = \sqrt{-1}$
j = photocurrent density, A cm^{-2}
j^H, j^{sc} = Faradaic current density, A cm^{-2}, at Helmholtz and semiconductor side, respectively
j_{sat} = saturated photocurrent density, A cm^{-2}
j_{ss} = current of charging the surface state capacitance, A cm^{-2}
j_{st} = steady-state photocurrent density, A cm^{-2}
k_i, i = 1−4, reaction rate constants
κ = Boltzmann constant, 1.38 $\times$ 10^{-23} J K^{-1}
n_s = electron density at the semiconductor surface, cm^{-2}
p = charge density, cm^{-2}
$p_1{}^0$ = steady-state free holes density at the surface, cm^{-2}
$p_2{}^0$ = steady-state holes density captured by surface states, cm^{-2}
q = element charge, 1.602 $\times$ 10^{-19} C
R = organic pollutants
R_s = solution resistance, Ω cm^{-2}
R_{ss} = resistance associated with surface state charging, Ω cm^{-2}
r = surface state density, cm^{-2}
T = absolute temperature
t = time, s
ω = angular frequency, s^{-1}
$Y_F(\omega)$ = faradaic admittance of photoelectrochemical system
$Z(\omega)$ = impedance of photoelectrochemical system, Ω cm^{-2}
ϕ = applied electrode potential, V

ϕ_H = potential drop across the Helmholtz layer, V
ϕ_{sc} = potential drop across the depletion layer, V
τ_{ss} = time constant of charging of surface states, s
$\sim$ = superscript denoting ac component

References and Notes

(1) Hoffman, M. R.; Martin, S. T.; Wonyong, C.; et al. *Chem. Rev.* **1995**, *19*, 69.
(2) Hidaka, H.; Asai, Y.; Jinchai, Z.; et al. *J. Phys. Chem.* **1995**, *99*, 8244.
(3) Vinodgopal, K.; Hotchandani, S.; Kamat, P. V. *J. Phys. Chem.* **1993**, *97*, 9040.
(4) Vinodgopal, K.; Stafford, U.; Gray, K. A.; Kamat, P. V. *J. Phys. Chem.* **1993**, *97*, 6797.
(5) Kesselman, J. M.; Shreve, G. A.; Hoffman, M. R.; et al. *J. Phys. Chem.* **1994**, *98*, 13385.
(6) Leng, W. H.; Zhang, Z.; Zhang, J. Q. *J. Mol. Catal. A*: *Chem.* **2003**, *206*, 239.
(7) Calvo, M. E.; Candal, R. J.; Bilmes, S. A. *Environ. Sci. Technol.* **2001**, *35*, 4132.
(8) Waldner, G.; Pourmodjib, M.; Bauer, R.; Neumann-Spallart, M. *Chemosphere* **2003**, *50*, 989.
(9) Jiang-Lin, C.; Wen-Hua, L.; Jian-Qing, Z.; Chun-Nan, C. *Acta Phys. Chin. Sin.* **2004**, *20*, 735.
(10) Hagfeldt, A.; Grätzel, M. *Chem. Rev.* **1993**, *93*, 671.
(11) Lewis, N. S. *J. Phys. Chem. B* **1998**, *102*, *4843*.
(12) (a) Nozik, A. J.; Memming, R. *J. Phys. Chem.* **1996**, *100*, 13061. (b) Lewis, N. S. *Acc. Chem. Res.* **1990**, *23*, 176. (c) Salvador, P. *J. Phys. Chem. B* **2001**, *105*, 6182. (d) Bisquert, J.; Zaban, A.; Greenshtein, M.; Mora-Sero, I. *J. Am. Chem. Soc.* **2004**, *126*, 13550. (e) Ahmed, S.; Fonseca, S. M.; Kemp, T. J.; Unwin, P. R. *J. Phys. Chem. B* **2003**, *107*, 5892. (f) Jin, Z. Z. *J. Phys. Chem. B* **2000**, *104*, 7239. (g) Nishida, M. *J. Appl. Phys.* **1980**, *51*, 1669. (h) Hagfeldt, A.; Björkstén, U.; Grätzel, M. *J. Phys. Chem.* **1996**, *100*, 8045. (i) Liao, K. H.; Waldeck, D. H. *J. Phys. Chem.* **1995**, *99*, 4569.
(13) Mandelbaum, P. M.; Regazzoni, A. E.; Blesa, M. A.; et al. *J. Phys. Chem. B* **1999**, *103*, 5505.
(14) De Jonh, P. E.; Vanmaekelbergh, D. *J. Phys. Chem. B* **1997**, *101*, 2716.
(15) Peter, L. M. *Chem. Rev.* **1990**, *90*, 753.
(16) Semenikhin, O. A.; Kazarinov, V. E.; Jiang, L.; et al. *Languir* **1999**, *15*, 3731.
(17) Oekermann, T.; Schlettwein, D.; Jaeger, N. I. *J. Phys. Chem. B* **2001**, *105*, 9524.
(18) Peat, R.; Peter, L. M. *J. Electroanal. Chem.* **1987**, *228*, 351.
(19) Cass, M. J.; Duffy, N. W.; Peter, L. M.; et al. *J. Phys. Chem. B* **2003**, *107*, 5857.
(20) Ponomarev, E. A.; Peter, L. M. *J. Electroanal. Chem.* **1995**, *397*, 45.
(21) Ponomarev, E. A.; Peter, L. M. *J. Electroanal. Chem.* **1995**, *396*, 219.
(22) Peter, L. M.; Ponomarev, E. A.; Fermín, D. J. *J. Electroanal. Chem.* **1997**, *427*, 79.
(23) Schefold, J. *J. Electrochem. Soc.* **1995**, *142*, 850.
(24) Bisquert, J.; Garcia-Belmonte, G.; Fabregat-Santiago, F.; et al. *J. Phys. Chem. B* **2000**, *104*, 2287.
(25) Liu, H.; Cheng, S. A.; Wu, M.; et al. *J. Phys. Chem.* A **2000**, *104*, 7016.
(26) Leng, W. H.; Zhang, Z.; Cheng, S. A.; et al. *Chin. Chem. Lett.* **2001**, *12*, 1019.
(27) Liu, H.; Li, X. Z.; Leng, Y. J.; Li, W. Z. *J. Phys. Chem. B* **2003**, *107*, 8988.
(28) Turchi, C. S.; Ollis, D. F. *J. Catal.* **1990**, *122*, 178.
(29) Fermin, D. J.; Ponomarev, E. A.; Peter, L. M. *J. Electroanal. Chem.* **1999**, *473*, 192.
(30) Hens, Z. *J. Phys. Chem. B* **1999**, *103*, 122.
(31) Cao, C. N.; Zhang, J. Q. *An Introduction to Electrochemical Impedance Spectroscopy*; Science Press: Beijing, China, 2002; pp 76−83.
(32) Moser, J.; Punchihewa, S.; Infelta, P. P.; Grätzel, M. *Langmuir* **1991**, *7*, 3012.
(33) Tunesi, S.; Anderson, M. A. *J. Phys. Chem.* **1991**, *95*, 3399.
(34) Weisz, A. D.; Rodenas, L. G.; Morando, P. J.; Regazzoni, A. E.; Blesa, M. A. *Catal. Today* **2002**, *76*, 103.
(35) Mandelbaum, P.; Bilmes, S. A.; Regazzoni, A. E.; Blesa, M. A. *Solar Energy* **1999**, *65*, 75.
(36) Regazzoni, A. E.; Mandelbaum, P.; Matsuyoshi, M.; Schiller, S.; Bilmes, S. A.; Blesa, M. A. *Langmuir* **1998**, *14*, 868.
(37) Morand, R.; Noworyta, K.; Augustynski, J. *Chem. Phys. Lett.* **2002**, *364*, 244.
(38) Calvo, M. E.; Candal, R. J.; Bilmes, S. A. *Catal. Today* **2002**, *76*, 133.
(39) Oskam, G.; Schmidt, J. C.; Hoffmann, P. M.; Searson, P. C. *J. Electrochem. Soc.* **1996**, *143*, 2531.
(40) Oskam, G.; Hoffmann, P. M.; Searson, P. C. *Phys. Rev. Lett.* **1996**, *76*, 1521.
(41) Cunningham, J.; Al-Sayyed, G.; Sedlak, P.; Caffrey, J. *Catal. Today* **1999**, *53*, 145.
(42) Kratochvilová, K.; Hoskovcová, I.; Jirkovský, J.; Klíma, J.; Ludvík, J. *Electrochim. Acta* **1995**, *40*, 2603.
(43) (a) Salvador, P. *J. Phys. Chem.* **1985**, *89*, 3863. (b) Ferrer, I. J.; Muraki, H.; Salvador, P. *J. Phys. Chem.* **1986**, *90*, 2805.
(44) Peter, L. M.; Li, J.; Peat, R. *J. Electroanal. Chem.* **1984**, *165*, 29.
(45) (a) Brown, G. T.; Darwent, J. R.; Fletcher, P. D. I. *J. Am. Chem. Soc.* **1985**, *107*, 6446. (b) Bahnemann, D.; Henglein, A.; Lilie, J.; Spanhel, L. *J. Phys. Chem.* **1984**, *88*, 709.